analytical chemistry

pubs.acs.org/ac Article

Aptamer Self-Assembly-Functionalized Nanochannels for Sensitive and Precise Detection of Chloramphenicol

Xu-Qin Ran, Hai-Long Qian, and Xiu-Ping Yan*

Cite This: *Anal. Chem.* 2021, 93, 14287−14292 Read Online

ACCESS | Metrics & More | Article Recommendations | Supporting Information

ABSTRACT: Sensitive and precise determination of chloramphenicol (CAP) is of great significance for human health due to its high risk in trace amounts. Solid-state artificial nanochannels are expected to be highly promising sensing devices owing to single-molecule sensitivity, target-specific selectivity, and portability. Herein, we report an aptamer self-assembly-functionalized artificial nanochannel-based sensor for highly sensitive and precise determination of CAP. Aptamer self-assembly (AAs) served as the specific recognition component and were in situ grown on the surface of stable anodic aluminum oxide (AAO) nanochannels to develop an AAs@AAO nanochannel-based sensor. Selective interaction with CAP led to the disassembly of AAs and sensitive current change of AAs@AAO nanochannels, allowing sensitive and precise sensing of CAP in complex food samples. The developed AAs@AAO nanochannel-based sensor showed a wide linear range from 0.32 to 1600 pg. mL^{-1}, low limit of detection (LOD) of 0.1 pg. mL^{-1}, high precision with relative standard deviation of 2.9%, and quantitative recoveries of 93.4−102.2% for CAP in milk, milk powder, and honey samples. This work proposes a versatile nanochannel-based platform for facile, sensitive, and precise sensing of hazardous residues in food samples.

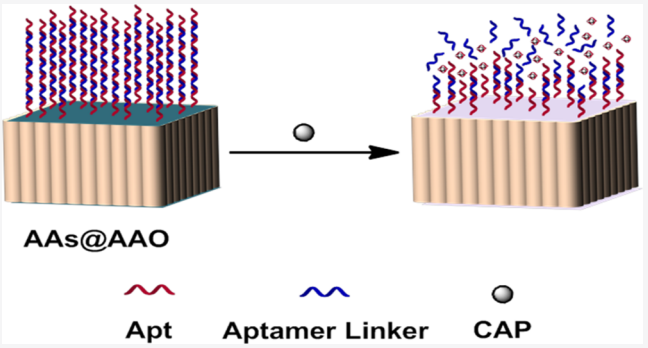

INTRODUCTION

As one of the common veterinary antibiotics, chloramphenicol (CAP) is widely utilized to treat infectious diseases including typhoid fever, cholera, and meninges.[1,2] Nevertheless, trace level residual of CAP in food likely leads to serious side effects to human such as aplastic anemia, kidney damage, nausea, and allergic reactions due to the bioconcentration of food chain.[3−5] The European Union defines the CAP as a prohibited substance in foodstuffs of animal origin. The risk management measure for CAP recommended by the Codex Alimentarius Commission is to not be used in food producing animals.[6,7] Therefore, sensitive and precise detection of CAP in food is of great significance to human health.

High-performance liquid chromatography (HPLC) and its combination with mass spectrometry (HPLC-MS) are considered to be general validated methods for CAP but are limited by the large equipment with professional laboratory conditions.[1,8−10] Fluorescence sensing is sensitive and simple but usually suffers from the autofluorescence interference from the sample matrix.[11] The antibody applied in an enzyme-linked immunosorbent assay is expensive and hardly accessible.[12] Therefore, the development of a facile, portable, and cost-effective method for sensitive and precise determination of CAP in food is indispensable.

Solid-state artificial nanochannels with good mechanical and chemical stability are promising sensing devices owing to single-molecule sensitivity, target-specific selectivity, and portability.[13−18] The transient ion current change can be sensitively measured when a single molecule passes through the nanochannels.[19−21] Moreover, the nanochannels can be functionalized with special probe molecules.[22,23] The change of the current−voltage ($I-V$) curves from the recognition of the analyte allows its sensitive measurement. So far, artificial nanochannels have been applied in the detection of protein, DNA, chiral molecules, disease markers, and so on.[16,24−27] The requirement of small equipment makes nanochannel systems' high potential as a facile, portable, and cost-effective platform for sensing.[28]

Anodic aluminum oxide (AAO) with array nanochannels has drawn increasing attraction owing to its high channel density and mechanical stability.[29] Aptamers are well known as an intelligent recognizer with high stability, low cost, and excellent specific affinity toward a target.[30] Aptamers can be further assembled into a concatemer with a large number of charges and multi-binding sites to provide a built-in amplification

Received: August 9, 2021
Accepted: September 26, 2021
Published: October 12, 2021

https://doi.org/10.1021/acs.analchem.1c03396
Anal. Chem. 2021, 93, 14287−14292

mechanism.[25,31,32] Thus, aptamer self-assembly (AAs)-functionalized AAO nanochannels are of great potential for sensing.

Herein, we show an aptamer self-assembly-functionalized nanochannel-based sensor for the sensitive and precise determination of CAP in food. AAO with stable, regular, and adjustable nanochannels is modified with (3-aminopropyl)-triethoxysilane (APTES) to obtain amino-functionalized AAO (AAO-NH_2), and then aldehyde CAP aptamer (Apt) is grafted onto AAO-NH_2 to give CAP aptamer-functionalized AAO (Apt-AAO). Further in situ self-assembly of Apt on Apt-AAO gives AAs-functionalized AAO (AAs@AAO). Selective interaction with CAP leads to the disassembly of Apt from AAs@AAO and sensitive charge and current change, allowing sensitive and precise determination of CAP in food.

EXPERIMENTAL SECTION

Materials and Reagents. AAO with nanochannels (diameter, 30 ± 5 nm; thickness, 60 ± 5 μm; channel density, *ca.* 2.8×10^{10} cm^{-2}) was from PuYuan (Hefei, China). APTES was from Aladdin (Shanghai, China). Hydrochloric acid (HCl, 36%−38%), acetone, ethanol, (hydroxymethyl)methyl aminomethane (Tris, 99%), sodium chloride (NaCl), magnesium chloride ($MgCl_2 \cdot 6H_2O$, 98%), sodium hydroxide (NaOH), and acetic acid were from Sinopharm (Shanghai, China). CAP, thiamphenicol, florfenicol, kanamycin, gentamicin sulfate, and a certified reference material MRM0197-1 (milk powder) were from Meizheng Group (Beijing, China). Apt (5′-CHO-ACTTCAGTGAGTTGTCCCACGGTCGGCGAGTCGG-TGGTAG-3′),[33] its corresponding aptamer linker (5′-TGGG-ACAACTCACTGAAGTCCTACCACCGACTCGCCGAC-3′), and the Cyanine5 (Cy5)-labeled aptamer were from Sangon (Shanghai, China). Ultrapure water applied in the work was from Wahaha (Hangzhou, China). Analytical grade chemicals with no further purification were used throughout the work.

Fabrication of the AAs@AAO Nanochannel-Based Sensor. Typically, AAO was ultrasonically cleaned in ethanol and water for 5 min, then immersed in 5% HCl for 60 s, and finally dried with a vacuum freeze drier. The cleaned AAO was modified with acetone solution of APTES (15%, v/v) for 8 h, then washed with acetone, and baked at 120 °C for 2 h to obtain AAO-NH_2. To immobilize Apt, AAO-NH_2 was put into a three-necked flask, vacuumed for 2 h, then reacted in Tris−HCl (10 mM, pH 8.0) containing 500 mM NaCl, 1 mM $MgCl_2$, and 1.5 μM Apt for 4 h under gentle shaking, rinsed with ultrapure water, and finally dried to get Apt-AAO. For the functionalization of AAs, Apt-AAO was also vacuumed for 2 h, then reacted in Tris−HCl (10 mM, pH 8.0) containing 500 mM NaCl, 1 mM $MgCl_2$, 1.5 μM Apt, and a 1.5 μM aptamer linker for 4 h under gentle shaking, then rinsed with ultrapure water, and finally dried to get AAs@AAO-1. Multi-assembly was performed to repeat the above procedure for *n* runs to get AAs@AAO-*n*.

Instrumentation. Agarose gel electrophoresis images were acquired on a Gel Doc XR+ gel image analyzing system (BIO-RAD, US) and DYY-8C electrophoresis system (Beijing, China). Scanning electron microscope (SEM) images were recorded on an SU8100 scanning electron microscope (Hitachi, Japan). Ultraviolet (UV) spectra were acquired on a UV-3600PLUS spectrophotometer (Shimadzu, Japan). Zeta potential was measured on a Nano ZS Zetasizer with 633 nm He−Ne laser (Malvern, UK). Confocal images were acquired on an FV3000 laser scanning confocal microscope (LSCM) (OLYMPUS, China) under excitation at 405 nm. Surface contact angle images were acquired on an OCA15EC video optical contact angle measuring instrument (DFE, Germany). X-ray photoelectron spectra (XPS) were acquired on an Axis supra X-ray photoelectron spectrometer (Kratos, UK).

Sample Preparation. Fresh milk, student nutrition milk powder, jujube honey, infant milk powder, ultrahigh-temperature processing milk, acacia honey, pasteurized milk, adult nutrition milk powder, and osmanthus honey were obtained from local supermarkets. The samples were pretreated according to Wang et al. with slight modifications.[11] The milk sample (2.5 g) was dispersed in ultrapure water (10 mL), adjusted to pH 4.6 with acetic acid (20%, v/v), and centrifuged at 10000 rpm for 15 min to remove the denatured proteins. The supernatant was adjusted to pH 7.0 with NaOH solution (1 M), filtered with a 0.22 μm filter membrane, and adjusted to volume in a 50 mL volumetric flask with ultrapure water for analysis. Milk powder samples including MRM0197-1 were pretreated as milk samples. The honey sample (2.5 g) was dispersed completely in ultrapure water (10 mL) and centrifuged at 10,000 rpm for 15 min. The supernatant was filtered with a 0.22 μm filter membrane and adjusted to volume in a 50 mL volumetric flask with ultrapure water for analysis.

Determination of CAP. The determination of CAP was performed on a laboratory-built nanochannel system consisting of a homemade flow system, a 2450 SourceMeter (Keithley, US), and a data acquisition system (Version 2.06, Keithley, US) (Figure 1). The flow system contained two cells made of

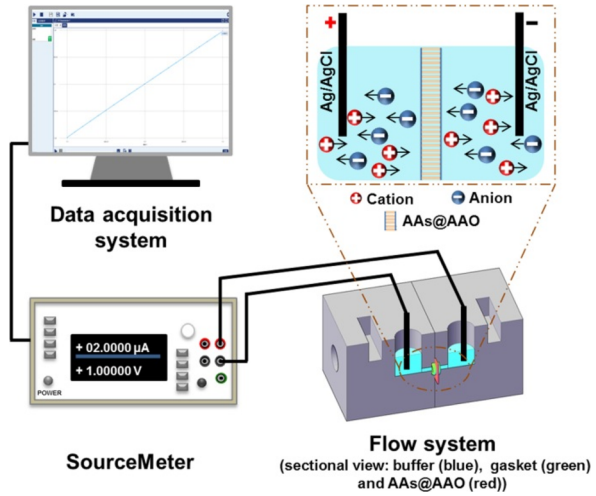

Figure 1. Schematic diagram for the laboratory-built nanochannel system.

polytetra fluoroethylene, and both cells were filled with Tris−HCl buffer (150 μL, 200 μM NaCl, pH 7.0). AAO was mounted between the two cells. The effective area for the ionic conductance measurement was 2.5 mm^2. An Ag/AgCl electrode was inserted to each cell to measure the transmembrane ionic current. The scan voltage from −1 to 1 V with a scan speed of 10 mV s^{-1} was applied. The standard solution of CAP or the prepared sample solution (40 μL) was incubated with AAs@AAO for 40 min, rinsed with the test buffer, and clamped in the flow system for analysis.

https://doi.org/10.1021/acs.analchem.1c03396
Anal. Chem. 2021, 93, 14287−14292

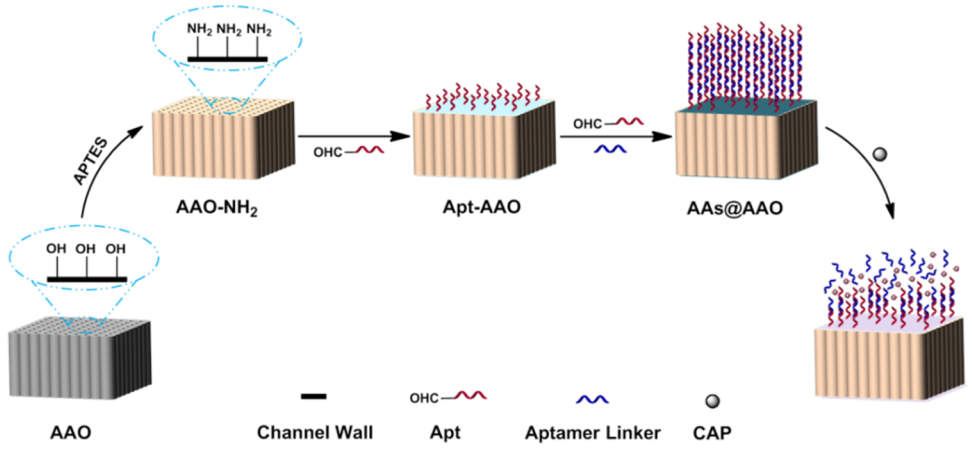

Figure 2. Illustration of the design and fabrication of the AAs@AAO nanochannel-based sensor for the detection of CAP.

RESULTS AND DISCUSSION

Design, Preparation, and Characterization of AAs@AAO. Figure 2 shows the design and preparation of the AAs-functionalized AAO nanochannel for the detection of CAP. We selected AAO to build the nanochannel system as the extremely high cylindrical channel density of AAO with stable, regular, and adjustable channels would facilitate sensitive current response.[30] AAO-NH_2 was first prepared by reacting APTES and the hydroxyl group in AAO. Then, the amino group of AAO-NH_2 was condensed with the aldehyde groups on the Apt via a Schiff-base reaction to form Apt-AAO. As AAs@AAO gives more charges and binding sites than Apt-AAO to promote the selectivity and sensitivity of the functionalized sensor,[32] the Apt and its target aptamer linker were further added to alternately hybridize each other to form AAs@AAO. The AAs would disassemble from AAs@AAO after selective interaction between CAP and its Apt, leading to sensitive change of the charge of AAs@AAO. As the result, the current of the AAs@AAO nanochannel-based sensor continuously change with CAP concentration, allowing the quantitative determination of CAP.

The prepared AAO-NH_2 was characterized by XPS, SEM, zeta potential, and contact angle experiments. The appearance of Si 2p and N 1s peaks in the XPS spectra of AAO-NH_2 confirms the successful modification of amino groups (Figure S1a,b). SEM images show that amino ($-NH_2$) functionalization with APTES did not significantly change the morphology and channel size of AAO (Figure S2a,b). The introduced positive charge with amino groups evidently increased the zeta potential of AAO-NH_2 (Figure 3a). The lower surface energy of AAO-NH_2 than that of AAO also reduced the hydrophilicity of the channel and increased the contact angle (Figure 3b).[34]

The effects of the concentration of Apt (0.1−2.0 μM) and reaction time (0−300 min) on the formation of Apt-AAO were investigated. To this end, the UV spectra of the supernatant after the reaction were monitored. No obvious absorption peak at 260 nm for Apt in the initial Apt concentration range from 0.1 to 0.8 μM demonstrates the complete graft of Apt on AAO (Figure S3). In contrast, the absorption peak for Apt started to appear in the supernatant as the initial concentration of Apt increased to 1.0 μM, indicating the excess Apt. To ensure the sufficient grafting of Apt, 1.5 μM Apt was used in the subsequent experiments. The absorption peak of Apt in the UV spectra of the supernatant decreased as the reaction time increased from 0 to 4 h. Further increase of the reaction time

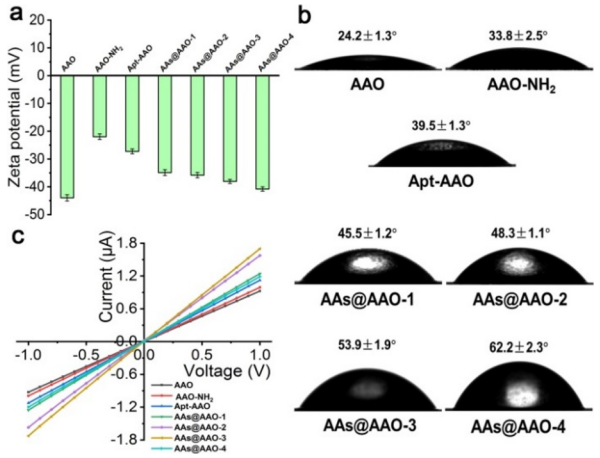

Figure 3. Characterization of the (a) zeta potential, (b) contact angle, and (c) $I-V$ curves for AAO, AAO-NH_2, Apt-AAO, AAs@AAO-1, AAs@AAO-2, AAs@AAO-3, and AAs@AAO-4.

gave no obvious change of the absorption peak of Apt, indicating that 4 h was sufficient for the reaction (Figure S4).

The evident appearance of P 2p peak in the XPS spectra of Apt-AAO indicates the successful grafting of Apt on the nanochannels (Figure S1c). The SEM image of Apt-AAO shows that the channels of AAO-NH_2 were a little bit covered after the reaction with Apt (Figure S2c). Owing to the negative charge and hydrophobicity of nucleobases, Apt-AAO gave a lower zeta potential of −27.2 eV and a larger contact angle of 39.5 ± 1.3° than those of AAO-NH_2 (−21.9 eV, 33.8 ± 2.5°, respectively) (Figure 3a,b).

The formation of AAs was first examined in solution by gel electrophoresis. The study on the effect of pH (5.0−10.0) shows that pH 8.0 is favorable for the formation of AAs (Figure S5). The increase of the concentration of NaCl from 50 to 400 mM facilitated the formation of AAs. Further increase of the concentration of NaCl to 600 mM gave no obvious improvement, so 500 mM NaCl was applied in this work (Figure S6). The pilot experiment for the disassembly of AAs with CAP was also conducted (Figure S7). The disappearance of a large molecular weight after the addition of CAP proves the successful disassembly of AAs. We further tried to in situ grow AAs on AAO under the above-obtained conditions. The evident decrease of the absorption peak of Apt in the UV spectra of the supernatant confirms the growth of

https://doi.org/10.1021/acs.analchem.1c03396
Anal. Chem. 2021, 93, 14287−14292

AAs on the AAO, indicating that the formation conditions of AAs in solution were also applicable for the growth of AAs on the AAO nanochannels (Figure S8).

The LSCM cross-sectional image of Cy5-labeled AAs@AAO shows the depth of AAs into the channel was *ca.* 1.5 μm (just 2.3% of the length of complete channel) and provides the proof of the external surface functionalization of AAs (Figure S9). Compared with the inner channel functionalization, the external modification of nanochannels possesses unique advantages for determination. The relatively free environment of the external surface receives less non-specific interference than the internal limited confined space. Additionally, the more accessible interaction of the analyte and the recognition component on the external surface of the channel enhances anti-interference ability in the complicated matrix.[25,35,36]

Multi-assembly of AAs@AAO-*n* was further performed to increase the charges and binding sites of functionalized AAs for selective and sensitive current response. SEM images clearly show the increase of AAs on AAO with an assembly run (Figure 4). After a four-run assembly, the AAs have already

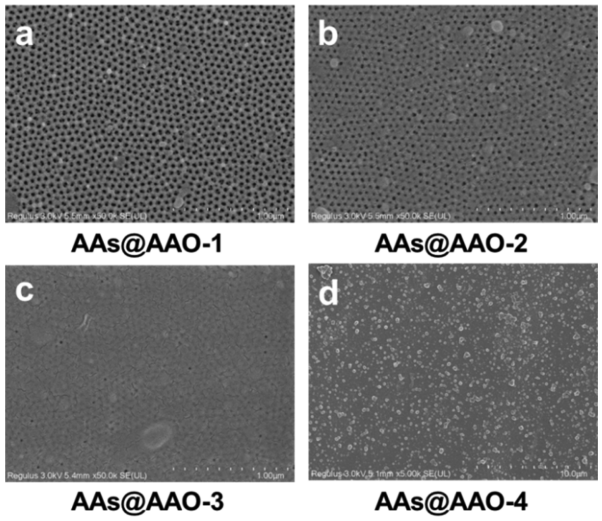

Figure 4. SEM images of AAs@AAO prepared with different assembly runs: (a) AAs@AAO-1; (b) AAs@AAO-2; (c) AAs@AAO-3; (d) AAs@AAO-4.

covered all the channels of AAO (Figure 4d). Additionally, the more negative zeta potential and larger contact angle of AAs@AAO after multi-assembly also indicate that more AAs were functionalized on the nanochannels (Figure 3a,b).

The effect of the assembly run on the *I*−*V* curve was investigated to obtain optimal AAs@AAO (Figure 3c). The functionalization of AAs did not change the symmetrical mass transfer behavior of the nanochannel based on the linear *I*−*V* curve of AAs@AAO-*n* and AAO (Figure S10).[37,38] The increase of the assembly run from 1 to 3 resulted in the evident enhancement of the current of AAs@AAO. Further increase to four runs led to the decrease of current due to the block of the ion transport channel with excessive AAs. In addition to charge, steric hindrance was involved in the influence of current response, which went against the selectivity and sensitivity.[39] No obvious change of the *I*−*V* curve of AAs@AAO-3 after 9 days indicates the good stability of the proposed sensor (Figure S11). Therefore, AAs@AAO-3 was employed for subsequent sensing.

Optimization of CAP Sensing. The effects of pH, NaCl concentration, and time on the specific disassembly of AAs caused by CAP were studied. Figure 5a shows that the current

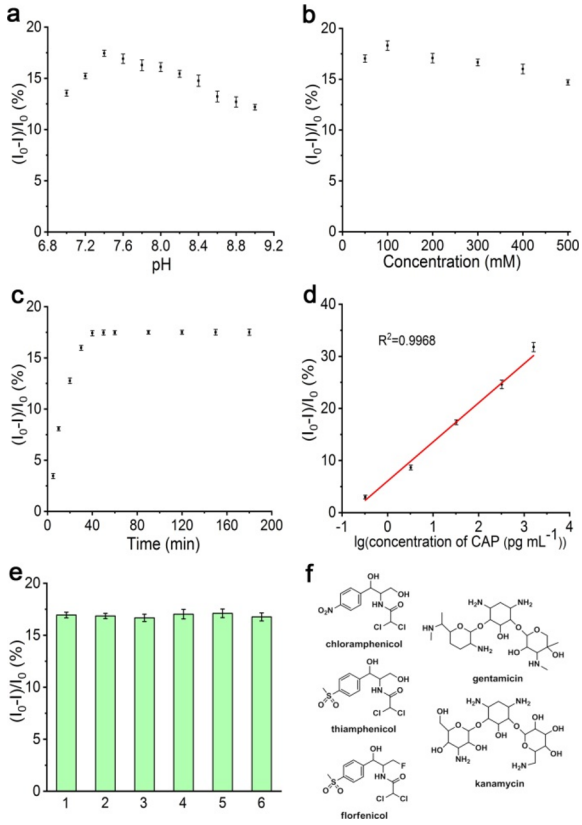

Figure 5. Effects of pH (a), NaCl concentration (b), and time (c) on the current decrease rate of the AAs@AAO-3 sensor in the presence of 32.3 pg. mL^{-1} CAP. (d) Calibration curve of the current decrease rate against the logarithm of CAP concentration in the range of 0.32−1600 pg. mL^{-1}. (e) Effects of other antibiotics (323.1 pg. mL^{-1}) on the current decrease rate of AAs@AAO-3 (1, CAP (32.3 pg. mL^{-1}); 2, CAP (32.3 pg. mL^{-1}) + thiamphenicol; 3, CAP (32.3 pg. mL^{-1}) + florfenicol; 4, CAP (32.3 pg. mL^{-1}) + kanamycin; 5, CAP (32.3 pg. mL^{-1}) + gentamicin; 6, CAP (32.3 pg. mL^{-1}) + thiamphenicol + florfenicol + kanamycin + gentamicin). (f) Chemical structures of CAP, thiamphenicol, florfenicol, kanamycin, and gentamicin.

decrease rate increased as pH increased to 7.4 and then decreased as pH further increased. Generally, the pH of solution changes the charge of the target and AAs due to the protonation/deprotonation process, thus affecting the non-covalent interactions between the aptamer and its target, such as van der Waals forces and electrostatic and hydrophobic interactions.[5]

In addition, NaCl influences electrostatic interaction, one of the main driving forces for the binding of the target and aptamer. The binding takes place with more difficulty at higher NaCl concentration.[5,40] As shown in Figure 5b, 100 mM NaCl gave the maximal current decrease rate. Sufficient time is also required for the target to disassemble AAs. Figure 5c shows that the current decrease rate significantly increased in the first 40 min, and kept stable after 40 min. On the basis of the above results, the optimal pH, NaCl concentration, and time were 7.4, 100 mM, and 40 min, respectively.

Figures of Merit for CAP Sensing. The analytical performance of the developed AAs@AAO-3 sensor was

https://doi.org/10.1021/acs.analchem.1c03396
Anal. Chem. 2021, 93, 14287−14292

evaluated under the optimal experimental conditions. The current exhibited an obvious decrease after the addition of CAP. The current change of AAs@AAO-3 due to the disassembly of AAs was highly related to the concentration of CAP, laying the foundation for the determination of CAP (Figure S12). A good linear calibration curve (the current decrease rate against the logarithm of the concentration of CAP) was obtained from 0.32 pg to 1600 pg mL^{-1} (R^2 = 0.9968) (Figure 5d). The developed method gave the detection limit (3 s) of 0.1 pg. mL^{-1} and the precision of 2.9% (RSD, n = 11) for 32.3 pg. mL^{-1} CAP. The wider linear range and lower detection limit of AAs@AAO-3 than AAs@AAO-1 indicate the efficiency of the multi assembly in improving the sensing performance (Table S1). The detection limit of the developed method for CAP is much lower than those of most previous methods, indicating its high potential for CAP determination (Table S2). In addition, the main used equipment of SourceMeter here is lower-priced than the common instruments used in other methods such as HPLC,[8] HPLC-MS,[3] Raman spectrometry,[41] and fluorescence spectrometry.[42] Therefore, the proposed nanochannel system is a promising cost-effective sensing platform.

Selectivity. To examine the selectivity of the proposed AAs@AAO sensor for CAP, the effects of other antibiotics including thiamphenicol, florfenicol, kanamycin, and gentamicin sulfate (Figure 5f) on the determination of CAP in a Tris−HCl buffer solution and food matrix (milk, milk powder, and honey) were studied. In the absence of CAP, there was no obvious change of the current decrease rate for the proposed AAs@AAO-3 sensor to other antibiotics (323.1 pg. mL^{-1}) (Figure S13 and S14). The recoveries of spiked Tris−HCl buffer for CAP (32.3 pg. mL^{-1}) in the presence of 323.1 pg. mL^{-1} antibiotics ranged from 97.5 to 104.5% (Table S3). Moreover, the addition of the 10 times higher concentration of the antibiotics with CAP in both Tris−HCl buffer and real samples gave little effect on the current decrease rate of the proposed AAs@AAO-3 sensor, indicating its high specificity for CAP (Figure 5e and Figure S15).

Validation and Application. Certified reference material MRM0197-1 was used to validate the proposed sensing method based on AAs@AAO-3. The concentration of CAP in MRM0197-1 was determined to be 0.81 ± 0.23 $\mu g\ kg^{-1}$ by the developed method, well agreeing with the certified value (0.83 ± 0.17 $\mu g\ kg^{-1}$) and confirming the accuracy of the developed method. Furthermore, the developed method was applied to determine CAP in real food samples (milk, milk powder, and honey). Only a fresh milk sample gave detectable CAP (0.133 ± 0.015 $\mu g\ kg^{-1}$). The recoveries of spiked CAP (0.5 $\mu g\ kg^{-1}$) in these samples were in range of 93.4−102.2%, further confirming the accuracy of the proposed method (Table 1).

Table 1. Analysis of Food Samples for CAP

samples	spiked CAP ($\mu g\ kg^{-1}$)	determined CAP ($\mu g\ kg^{-1}$) (mean ± s, n = 3)	recovery (%) (mean ± s, n = 3)
fresh milk	0	0.133 ± 0.015	
	0.5	0.609 ± 0.021	95.2 ± 2.2
ultrahigh-temperature processing milk	0	ND[a]	
	0.5	0.507 ± 0.009	101.4 ± 3.6
pasteurized milk	0	ND	
	0.5	0.482 ± 0.018	96.4 ± 4.3
infant milk powder	0	ND	
	0.5	0.503 ± 0.031	100.6 ± 2.9
acacia honey	0	ND	
	0.5	0.511 ± 0.044	102.2 ± 5.7
adult nutrition milk powder	0	ND	
	0.5	0.477 ± 0.017	95.4 ± 4.8
osmanthus honey	0	ND	
	0.5	0.467 ± 0.032	93.4 ± 2.3
student nutrition milk powder	0	ND	
	0.5	0.483 ± 0.026	96.6 ± 3.5
jujube honey	0	ND	
	0.5	0.509 ± 0.023	101.8 ± 6.4

[a]ND: not detected.

CONCLUSIONS

We have developed an aptamer self-assembly-functionalized nanochannel-based sensor for precise determination of CAP. The AAs was in situ grown on the external surface of AAO as a selective recognition unit to produce the AAs@AAO-based sensor. The current response of AAs@AAO to CAP realized the highly sensitive and precise detection of CAP. The developed method is easy to expand to other analytes by replacing AAs and shows promise as a versatile platform for the precise determination of hazardous residues in food.

ASSOCIATED CONTENT

Supporting Information

The Supporting Information is available free of charge at https://pubs.acs.org/doi/10.1021/acs.analchem.1c03396.

Additional figures and tables as described in the text; characterization of AAO with different groups (XPS, SEM, UV absorption spectra); gel electrophoresis images for AAs in solution; LSCM cross-sectional image of AAs@AAO; I−V curves of AAO with different groups; comparison of sensing performance of AAs@AAO-1 and AAs@AAO-3; comparison of the developed sensor with other reported methods; recoveries for the determination of CAP in the presence of other antibiotics (PDF)

AUTHOR INFORMATION

Corresponding Author

Xiu-Ping Yan − *State Key Laboratory of Food Science and Technology, International Joint Laboratory on Food Safety, Institute of Analytical Food Safety, School of Food Science and Technology, and Key Laboratory of Synthetic and Biological Colloids, Ministry of Education, Jiangnan University, Wuxi 214122, China;* orcid.org/0000-0001-9953-7681; Email: xpyan@jiangnan.edu.cn

Authors

Xu-Qin Ran − *State Key Laboratory of Food Science and Technology, International Joint Laboratory on Food Safety, and Institute of Analytical Food Safety, School of Food Science and Technology, Jiangnan University, Wuxi 214122, China*

Hai-Long Qian − *State Key Laboratory of Food Science and Technology, International Joint Laboratory on Food Safety, and Institute of Analytical Food Safety, School of Food*

https://doi.org/10.1021/acs.analchem.1c03396
Anal. Chem. 2021, 93, 14287−14292

Science and Technology, Jiangnan University, Wuxi 214122, China; orcid.org/0000-0001-7554-4115

Complete contact information is available at: https://pubs.acs.org/10.1021/acs.analchem.1c03396

Notes

The authors declare no competing financial interest.

■ ACKNOWLEDGMENTS

This work was supported by the National Natural Science Foundation of China (nos. 21775056 and 21804055), the National First-class Discipline Program of Food Science and Technology (no. JUFSTR 20180301), and the Program of "Collaborative Innovation Center of Food Safety and Quality Control in Jiangsu Province".

■ REFERENCES

(1) Mehlhorn, A.; Rahimi, P.; Joseph, Y. *Biosensors* **2018**, *8*, 54.
(2) Pilehvar, S.; Mehta, J.; Dardenne, F.; Robbens, J.; Blust, R.; De Wael, K. *Anal. Chem.* **2012**, *84*, 6753−6758.
(3) Kikuchi, H.; Sakai, T.; Teshima, R.; Nemoto, S.; Akiyama, H. *Food Chem.* **2017**, *230*, 589−593.
(4) Chang, H.; Lv, J.; Zhang, H.; Zhang, B.; Wei, W.; Qiao, Y. *Biosens. Bioelectron.* **2017**, *87*, 579−586.
(5) Khoshbin, Z.; Verdian, A.; Housaindokht, M. R.; Izadyar, M.; Rouhbakhsh, Z. *Biosens. Bioelectron.* **2018**, *122*, 263−283.
(6) Council Regulation. *Pharmacologically active substances and their classification regarding maximum residue limits in foodstuffs of animal origin*; No 37/2010; European Union (EU) Commission Regulation, 2010.
(7) Alimentarius Commission. *Maximun residue limits (MRLs) and risk management recommendations (RMRs) for residues of veterinary drugs in foods*; CAC/MRL 2−2015; Codex Alimentarius Commission, 2015.
(8) Huang, S.; Gan, N.; Liu, H.; Zhou, Y.; Chen, Y.; Cao, Y. *J. Chromatogr., B* **2017**, *1060*, 247−254.
(9) Yan, L.; Luo, C.; Cheng, W.; Mao, W.; Zhang, D.; Ding, S. *Electroanal. Chem.* **2012**, *687*, 89−94.
(10) Wu, Y.-Y.; Liu, B.-W.; Huang, P.; Wu, F.-Y. *Anal. Bioanal. Chem.* **2019**, *411*, 7511−7518.
(11) Wang, B.-B.; Zhao, X.; Chen, L.-J.; Yang, C.; Yan, X.-P. *Anal. Chem.* **2021**, *93*, 2589−2595.
(12) Wu, S.; Zhang, H.; Shi, Z.; Duan, N.; Fang, C.; Dai, S.; Wang, Z. *Food Control* **2015**, *50*, 597−604.
(13) Zhao, X.; Zhao, Y.; Deng, Y.; Zhou, D.; Zhang, Z.; Huang, Q.; Wang, D.-Q. *J. Micro-Bio Rob.* **2018**, *14*, 35−40.
(14) Yu, R.-J.; Ying, Y.-L.; Gao, R.; Long, Y.-T. *Angew. Chem., Int. Ed.* **2019**, *58*, 3706−3714.
(15) Lu, S.-M.; Peng, Y.-Y.; Ying, Y.-L.; Long, Y.-T. *Anal. Chem.* **2020**, *92*, 5621−5644.
(16) Boussouar, I.; Chen, Q.; Chen, X.; Zhang, Y.; Zhang, F.; Tian, D.; White, H. S.; Li, H. *Anal. Chem.* **2017**, *89*, 1110−1116.
(17) Lin, K.; Lin, C.-Y.; Polster, J. W.; Chen, Y.; Siwy, Z. S. *J. Am. Chem. Soc.* **2020**, *142*, 2925−2934.
(18) Pérez-Mitta, G.; Toimil-Molares, M. E.; Trautmann, C.; Marmisollé, W. A.; Azzaroni, O. *Adv. Mater.* **2019**, *31*, 1901483.
(19) Howorka, S.; Siwy, Z. *Chem. Soc. Rev.* **2009**, *38*, 2360−2384.
(20) Feng, Y.; Zhang, Y.; Ying, C.; Wang, D.; Du, C. *Genomics Proteomics Bioinf.* **2015**, *13*, 4−16.
(21) Han, C.; Hou, X.; Zhang, H.; Guo, W.; Li, H.; Jiang, L. *J. Am. Chem. Soc.* **2011**, *133*, 7644−7647.
(22) Pérez-Mitta, G.; Peinetti, A. S.; Cortez, M. L.; Toimil-Molares, M. E.; Trautmann, C.; Azzaroni, O. *Nano Lett.* **2018**, *18*, 3303−3310.
(23) Long, Z.; Zhan, S.; Gao, P.; Wang, Y.; Lou, X.; Xia, F. *Anal. Chem.* **2018**, *90*, 577−588.
(24) Zhao, X.-P.; Liu, F.-F.; Hu, W.-C.; Younis, M. R.; Wang, C.; Xia, X.-H. *Anal. Chem.* **2019**, *91*, 3582−3589.
(25) Ma, Q.; Li, Y.; Wang, R.; Xu, H.; Du, Q.; Gao, P.; Xia, F. *Nat. Commun.* **2021**, *12*, 1573.
(26) Ma, Q.; Si, Z.; Li, Y.; Wang, D.; Wu, X.; Gao, P.; Xia, F. *TrAC, Trends Anal. Chem.* **2019**, *115*, 174−186.
(27) Qiao, Y.; Qian, Y.; Liu, M.; Liu, N.; Tang, X. *Chem. Res. Chin. Univ.* **2019**, *35*, 837−841.
(28) Nie, G.; Sun, Y.; Zhang, F.; Song, M.; Tian, D.; Jiang, L.; Li, H. *Chem. Sci.* **2015**, *6*, 5859−5865.
(29) Rajeev, G.; Prieto Simon, B.; Marsal, L. F.; Voelcker, N. H. *Adv. Healthcare Mater.* **2018**, *7*, 1700904.
(30) Kurup, C.-P.; Tlili, C.; Zakaria, S.-N.-A.; Ahmed, M.-U. *Biointerface Res. Appl. Chem.* **2021**, *11*, 14057−14077.
(31) Liu, N.; Huang, F.; Lou, X.; Xia, F. *Sci. China Chem.* **2016**, *60*, 311−318.
(32) Liu, N.; Jiang, Y.; Zhou, Y.; Xia, F.; Guo, W.; Jiang, L. *Angew. Chem., Int. Ed.* **2013**, *52*, 2007−2011.
(33) Mehta, J.; Van Dorst, B.; Rouah-Martin, E.; Herrebout, W.; Scippo, M. L.; Blust, R.; Robbens, J. *J. Biotechnol.* **2011**, *155*, 361−369.
(34) Chai, C.; Lee, J.; Park, J.; Takhistov, P. *Appl. Surf. Sci.* **2012**, *263*, 195−201.
(35) Gao, P.; Ma, Q.; Ding, D.; Wang, D.; Lou, X.; Zhai, T.; Xia, F. *Nat. Commun.* **2018**, *9*, 4557.
(36) Li, X.; Zhai, T.; Gao, P.; Cheng, H.; Hou, R.; Lou, X.; Xia, F. *Nat. Commun.* **2018**, *9*, 40.
(37) Jiang, Y.; Feng, Y.; Su, J.; Nie, J.; Cao, L.; Mao, L.; Jiang, L.; Guo, W. *J. Am. Chem. Soc.* **2017**, *139*, 18739−18746.
(38) Siwy, Z. S. *Adv. Funct. Mater.* **2006**, *16*, 735−746.
(39) Pan, M.; Cai, J.; Li, S.; Xu, L.; Ma, W.; Xu, C.; Kuang, H. *Anal. Chem.* **2021**, *93*, 4825−4831.
(40) Lin, P.-H.; Yen, S.-L.; Lin, M.-S.; Chang, Y.; Louis, S. R.; Higuchi, A.; Chen, W.-Y. *J. Phys. Chem. B.* **2008**, *112*, 6665−6673.
(41) Yan, W.; Yang, L.; Zhuang, H.; Wu, H.; Zhang, J. *Biosens. Bioelectron.* **2016**, *78*, 67−72.
(42) Zhang, S.; Ma, L.; Ma, K.; Xu, B.; Liu, L.; Tian, W. *ACS Omega* **2018**, *3*, 12886−12892.